

Simultaneous Two-Dimensional Determination of Mixture Fraction and Flow-Velocity in a Non-Reacting Free Jet Flow by Planar LIF and PIV

Sebastian Pfadler^{1,*}, Micha Löffler¹, Friedrich Dinkelacker², Frank Beyrau¹ and Alfred Leipertz¹

1: Lehrstuhl für Technische Thermodynamik, University of Erlangen-Nürnberg, Erlangen, Germany

2: Lehrstuhl für Thermodynamik und Verbrennung, University of Siegen, Siegen, Germany

*: Corresponding author, e-mail: sp@ltt.uni-erlangen.de

Abstract In this study we present an experimental approach to the simultaneous two-dimensional measurement of mixture fraction and flow velocity in a non-reacting jet flow. For this, planar laser-induced fluorescence (LIF) and particle image velocimetry (PIV) have been applied simultaneously. The aim of this work is to provide data for the validation of models used in large eddy simulations (LES) which require measurements both of quantities on a subgrid level and of spatially filtered quantities. Therefore, a high spatial resolution for both measurement techniques has been used.

Beside the resulting experimental challenge to measure the two-dimensional flow field of a jet flow with large velocities ($Ma \approx 0.2$) in very small regions of interest with a distance between adjacent vectors of almost 100 μm , a quantitative measurement technique for the simultaneous determination of the mixture fraction is developed.

The applied experimental setup consisted of a central nozzle from where air is expanded isothermally with high outlet velocities into a slowly moving co-flow. Here, a gaseous fluorescence tracer in negligible concentration is added to the central flow in order to measure the mixture fraction directly from the number-density dependent laser-induced fluorescence signal. Different measures, e.g., the application of an optical beam homogenizer, were taken in order to exclude influences like temporal fluctuations and spatial distributions of the laser intensity which could have a negative effect on the quantitative evaluation.

The simultaneous measurement of mixture fraction and the flow field with high resolution allows to acquire appropriate data sets for comparison with LES. Here, the scales below the filter size Δ , where models are used to describe the transport mechanisms, are accessible from the high resolution measurements, whereby the filtered large scale structures are derived from spatially averaging some adjacent regions of interest.

This enabled us for the first time to the best of our knowledge, to measure directly the so called subgrid scale (SGS) scalar flux, which is usually modeled with standard gradient approaches in conjunction with the Smagorinsky-model for the subgrid scale turbulent viscosity ν_t .

Exemplary, measured data are presented for a non-reacting jet-flow for a Reynolds numbers of 31714.

1. Introduction

Turbulent mixing processes are characterized by a large bandwidth of time and length scales. This can be shown in form of the energy spectrum for scalar fluctuations (Hinze, 1962). The energy of these fluctuations is injected by convective processes at large structures (small wavenumbers), which are inherently anisotropic. The energy is successively transported towards larger wavenumbers by turbulent transport until a dissipation of the scalar fluctuation is effected by molecular diffusion.

However, the importance of large-scale structures for mixing of different species is evident from their considerable contribution to the total mass and energy transport.

Thus, for modeling purposes in the frame of computational fluid dynamics (CFD), strategies should be followed which account as well for large structures (convection) as for diffusive effects. In this context, the influence of large eddy simulation (LES) techniques has gained higher significance within the last decade.

Although the required computational power and time ranges between direct numerical simulation

(DNS), where all time and length scales are resolved, and the widespread Reynolds averaged Navier-Stokes approaches (RANS), being characterized by a high degree of modeling influences, LES allegorizes a promising approach for the numerical calculation of turbulent flows.

Therefore, LES has achieved a high development status for the simulation of non-reacting flows in the past, which is more and more expanding towards the modeling of reactive flows.(see, e.g., Cook, et al., 1998; Pitsch, et al., 2000). A good overview of the state-of-the-art is given in Meneveau, et al. (2000) and Steiner, et al. (2001). However, further strategies for the modeling of scalar transport are required, strongly demanding experimental sources for verification.

Basically, the approach of LES is the explicit computation of structures which are larger than a certain filter-size Δ , which has to be fixed prior to calculation, in combination with modeling of the finer structures. Thus, the inherent properties of instationarity and three-dimensionality are considered. This enables flow calculations of highly turbulent flows with significantly increased accuracy in principle, which is not possible with the commonly used RANS approach.

In LES, the governing equations are obtained by applying a spatial filter to the balance equations of fluid mechanics.

In Eq. (1), $\bar{\phi}$ denotes the filtered or large scale part of a flow variable ϕ , where D is the flow domain and G the convolution kernel of the applied filter. In compressible and reactive flows with

$$\bar{\phi}(x) = \int_D \phi(x') G_\Delta(x, x') dx' \quad (1)$$

strongly varying densities, filtered density- or Favre weighted quantities $\tilde{\phi} = \overline{\rho\phi}/\bar{\rho}$ need to be defined.

Besides the filtered continuity- and momentum conservation equation (Eqs. (2) and (3)) also filtered equations of the passive or reacting scalars have to be solved.

$$\frac{\partial \bar{\rho}}{\partial t} + \frac{\partial}{\partial x_i} (\bar{\rho} \tilde{u}_i) = 0 \quad (2)$$

$$\frac{\partial \bar{\rho} \tilde{u}_i}{\partial t} + \frac{\partial}{\partial x_j} (\bar{\rho} \tilde{u}_i \tilde{u}_j) = \frac{\partial}{\partial x_j} \left(\bar{\rho} \tilde{v} \left(\frac{\partial \tilde{u}_i}{\partial x_j} + \frac{\partial \tilde{u}_j}{\partial x_i} \right) - \frac{2}{3} \bar{\rho} \tilde{v} \frac{\partial \tilde{u}_k}{\partial x_k} \delta_{ij} + \bar{\rho} \tau_{ij}^{SGS} \right) - \frac{\partial \tilde{p}}{\partial x_i} \quad (3)$$

As an example for a passive scalar, the resulting conservation equation for the mixture fraction f (Chen, et al., 1990) is given in Eq. (5). It is defined in terms of the dimensionless mass fraction y_i of a certain species compared to reference conditions, ranging from 0 to 1 (see Eq. (4) for the simplified case of mixing of pure substances). In the field of combustion modeling, f can be described as a dimensionless fuel concentration.

$$f = \frac{y_i}{y_{i,0}} \quad (4)$$

$$\frac{\partial \bar{\rho} \tilde{f}}{\partial t} + \frac{\partial (\bar{\rho} \tilde{u}_i \tilde{f})}{\partial x_i} = \frac{\partial}{\partial x_i} \left(\bar{\rho} \tilde{D} \frac{\partial \tilde{f}}{\partial x_i} + \bar{\rho} J_i^{SGS} \right) \quad (5)$$

Due to the nonlinearity of the convective term, Eqs. (3) and (5) contain unknown terms, namely the subgrid scale stress τ_{ij}^{SGS} and the subgrid scale scalar flux J_i^{SGS} , respectively (Wegner, et al., 2002).

The anisotropic part of the SGS stress tensor is described with an eddy-viscosity assumption by employing a standard Smagorinsky model (Smagorinsky, 1963) (Eq. (6a)), whereas the isotropic part is included in the pressure term.

$$\tau_{ij}^{SGS} - \frac{1}{3} \delta_{ij} \tau_{kk} \approx 2\nu_t \widetilde{S}_{ij} \quad \text{(a)} \quad \nu_t = (C_s \Delta)^2 |\widetilde{S}_{ij}| \quad \text{(b)} \quad \widetilde{S}_{ij} = \frac{1}{2} \left(\frac{\partial \widetilde{u}_i}{\partial x_j} + \frac{\partial \widetilde{u}_j}{\partial x_i} \right) = \begin{pmatrix} S_{11} & S_{12} & S_{13} \\ S_{21} & S_{22} & S_{23} \\ S_{31} & S_{32} & S_{33} \end{pmatrix} \quad \text{(c)} \quad (6)$$

In Eqs. (6a-c), ν_t is the turbulent viscosity, C_s denotes a modeling constant which is obtained from following an approach suggested by Lilly (1992) and S_{ij} is the deformation tensor.

The SGS scalar flux of the mixture fraction f is closed by the eddy viscosity model, assuming a constant relationship between the turbulent diffusion coefficient D_t and the turbulent viscosity ν_t , being characterized by the turbulent Schmidt-number $Sc_t = \nu_t / D_t$. Following the simple standard gradient approach for turbulent transport, the SGS scalar flux can be formulated as

$$J_i^{SGS} = \widetilde{u}_i \widetilde{f} - \widetilde{u}_i \widetilde{f} \approx -D_t \frac{\partial \widetilde{f}}{\partial x_i} = -\frac{\nu_t}{Sc_t} \frac{\partial \widetilde{f}}{\partial x_i}. \quad (7)$$

In the past, this approach has found to give acceptable results on the field of combustion modeling (Branley, et al., 2001; Forkel, et al., 2000; Jaber, et al., 2003; Jimenez, et al., 2000; Kerstein, 1988; Pitsch, et al., 2000; Speziale, et al., 1988; Stolz, et al., 1999). However, several other approaches were developed, as the gradient model suffers from the assumption of a constant Schmidt-number and a restricted transport along the scalar gradient.

So far, a detailed analysis of the models has been performed mainly based on DNS data with simplified geometries for Reynolds numbers up to 10000. However, of more practical interest are complex flows at high Reynolds numbers. These flows feature strong inhomogeneities combined with anisotropic processes, which are not considered in the existing approaches, being based on isotropic assumptions. Therefrom a further model improvement and the need for validation arises, which is mainly restricted by the unavailability of suitable experimental data.

In this context, this article describes an experimental approach for the simultaneous two-dimensional measurement of mixture fraction and flow velocity in a non-reacting jet flow with the aim to provide data for the validation of models used in large eddy simulations, especially for the direct measurement of the SGS scalar flux.

2. Experimental

2.1 Strategy for simultaneous filtered- and SGS measurements

The aim of the presented experimental approach is to provide data for comparisons with LES studies. This is closely connected with the provision of spatially filtered quantities, like spatially averaged velocity components or mixture fraction at different downstream positions of the jet flow. Directly linked with the need to assess the quality of the models for closure of the SGS scalar transport, measurements have to be performed simultaneously both above the filtersize Δ and on the sub-grid level, where ideally even the smallest scales should be resolved.

Therefore, the resolution of the measurements is adjusted to provide the highest possible spatial resolution between adjacent regions of interests (ROIs) with the aim to gain filtered quantities via spatially averaging the finest measurable scales. The latter are regarded to resolve the flow-field adequately for the comparative analysis of SGS model predictions. In Fig. 1, the spatial averaging procedure over the smallest measurable scales is shown.

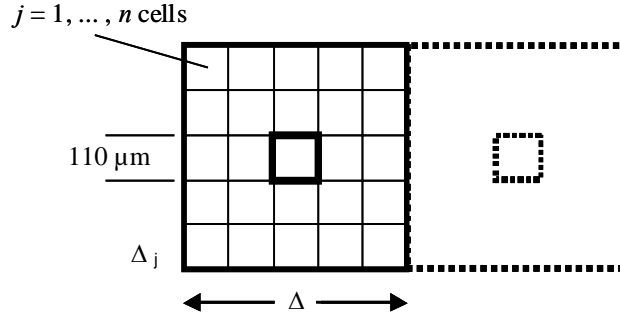


Fig. 1. Spatial averaging of directly measured sub-scale quantities

In this study, the spatial filtering over an area of Δ^2 included 81 SGS values with an individual spacing of $110 \mu\text{m}$, resulting in a filter width of 1 mm . The practical filtering is performed by forming the arithmetic mean value over the number n of measured SGS quantities inside the area with the border length Δ , see Eqs. (8 a-c):

$$\overline{u_i} = \frac{1}{n} \sum_{j=1}^n u_{i,j} \quad (\text{a}) \quad \overline{f} = \frac{1}{n} \sum_{j=1}^n f_j \quad (\text{b}) \quad \overline{u_i f} = \frac{1}{n} \sum_{j=1}^n u_{i,j} \cdot f_j \quad (\text{c}) \quad (8)$$

Subsequent to the spatial filtering of the instantaneous images, ensemble averages of the filtered quantities (typically 512 single shots) were calculated, denoted by brackets “ $\langle \rangle$ ”. Therefrom, filtered instantaneous fluctuations $\overline{\phi}'$ as well as ensemble averaged RMS-fluctuations $\overline{\phi}^{RMS}$ were derived, see Eq. (9).

$$\overline{\phi}^{RMS} = \sqrt{\langle \overline{\phi}'^2 \rangle} = \sqrt{\frac{1}{N} \sum_{n=1}^N (\langle \overline{\phi} \rangle - \phi_n)^2} \quad \text{with} \quad \langle \phi \rangle = \frac{1}{N} \sum_{n=1}^N \phi_n \quad (9)$$

For a better comparison between calculated and measured turbulence field, filtered correlation coefficients $\overline{R_{ij}}(r)$ of velocity components u_i and the mixture fraction f were derived from the spatially filtered instantaneous fluctuations (Eq. (10)). For details about gaining spatial correlation coefficients from an ensemble of planar measurements see, e.g., Pfadler, et al. (2005).

$$\overline{R_{ij}}(r) = \frac{\langle \overline{\phi}'_i(x) \cdot \overline{\phi}'_j(x + \Delta r) \rangle}{\overline{\phi}'_i(x) \cdot \overline{\phi}'_j(x)} \quad (10)$$

Here, auto-correlations of axial velocity and mixture fraction were performed in radial direction, starting at the burner central axis for different downstream positions. For the case of correlating the spatially filtered axial velocity fluctuations along the radial direction, the correlation is called transversal correlation.

In order to directly measure the SGS scalar flux in axial and radial direction, the individual terms of Eq. (7) are first spatially filtered and afterwards averaged over the ensemble of the single shot measurements.

2.2 Experimental set-up

Free jet geometry

The flow configuration investigated in this study is identical to that suggested at the 1st International Workshop on Measurements and Computation of Turbulent Nonpremixed Flames in Napoli (1996). This geometry was investigated by different groups in several studies before and a number of data-sets are already existent, being mainly directed for comparisons with numerical RANS studies.

Here, a free jet of pure air with a nozzle diameter of 8 mm is embedded into a concentric air co-flow with an inner diameter of 140 mm. It expands at 989 mbar and 301.15 K into ambient air (see Fig. 2). The mean outlet velocity of the inner jet is adjusted to be 64.5 m/s ($Re=31714$), whereas the mean velocity of the co-flow was chosen to be 0.3 m/s. The resulting total mass flow-rates were controlled via digital mass flow controllers with special calibration accuracy to grant highest possible reproducibility and accuracy.

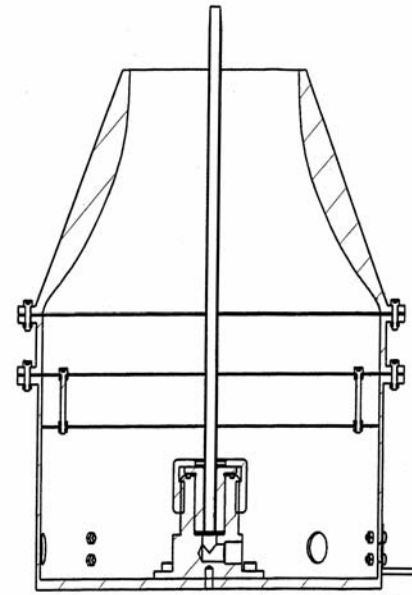


Fig. 2. Burner geometry

PIV experiment

Particle image velocimetry was applied to characterize the flow field with high spatial resolution. Therefore, the emitted light from two separate frequency doubled Nd:YAG lasers was superposed by a polarizing beam splitter cube and formed to a light-sheet of $\sim 100 \mu\text{m}$ thickness by a combination of plano-convex cylindrical lenses. The object plane, which is located at the burner central axis, is imaged onto the CCD-chip of a double-shutter camera by a $f=135\text{mm}$ Nikon Nikkor objective ($f/2.0$), with the magnification being adjusted by extension rings to achieve highest possible resolution. The camera was mounted on a Scheimpflug adapter in order to compensate for defocussing of the image plane which is caused by the oblique viewing angle of 30° (the camera for the LIF experiment is mounted perpendicular to the lightsheet). Di-ethyl-hexyl-sebacat (DEHS) droplets with an average diameter of $1 \mu\text{m}$ were seeded to the central jet as well as to the co-flow by two Laskin nozzle aerosol generators, being fed by mass-flow controllers. The single images from the Mie-scattering on the droplets, which are recorded within an interval of $1.4 \mu\text{s}$, are cross-correlated by using adaptive multi-passing techniques with a final overlap of adjacent regions of interest (ROIs) of 50 % (initial ROI size: 64×64 , final ROI size: 16×16). Resulting from the properties of the jet flow to have high gradients in the total velocity, special evaluating techniques had to be applied. In order to gain high vector yield by suppressing correlation noise, especially inside the instantaneous shear layer, 2nd order correlation techniques were applied (Hart, 1998). As a result, erroneous vectors were minimized, whereby post-processing steps could be reduced to the application of a filter, only restricting the allowed vector range. Filtered vectors were interpolated by their neighbors. Furthermore, for the last correlation step of the multi-pass correlation procedure, a normalized correlation function (Ronneberger, et al., 1998) was applied. Thus, the different seeding densities between the central jet and the co-flow were accounted for.

LIF experiment

Simultaneously to the measurement of the flow field, the instantaneous mixture fraction field of the jet was investigated by quantitative laser-induced fluorescence of a gaseous tracer added to the central flow (TLIF). Hereby, the mixture fraction is evaluated in terms of maximum concentration of the traced inner jet flow, where it is defined to be $f=1$.

In general, the quantification process of laser-induced fluorescence techniques applied to experimental fluid flows is influenced by several factors.

On the one hand quenching processes of the fluorescing molecules can make the quantification difficult if the dependency of the detectable signal on the quenching partners, temperature and pressure is unknown or cannot be calibrated for. On the other hand, fluctuations of the spatial intensity distribution of the applied laser system can increase the total error of the measurement, as normalization to known reference conditions cannot completely compensate beam inhomogeneities. These influences have been avoided in the described measurement as will be described subsequently, so that the measurement of the mixture fraction in terms of the inner flow could be performed quantitatively.

The influence of fluorescence quenching was avoided since both the inner jet as well as the surrounding co-flow feature the same molecular composition. Therefore, the detectable signal, which is shown to be located in the linear regime of laser induced fluorescence, is only a function of the number density of the tracer molecules, if the incident laser energy is constant. The latter was logged by a whole field energy meter and each individual image was normalised by the incident laser pulse energy.

Beam inhomogeneities, which are typical for unstable resonator excimer lasers were corrected by applying an optical beam homogenizer to the directly emitted laser light. The remaining inhomogeneities which are caused by interference phenomena are less than $\pm 5\%$. Moreover, the spatial fluctuations are significantly reduced, what depicts a basic requirement for quantitative planar laser diagnostics.

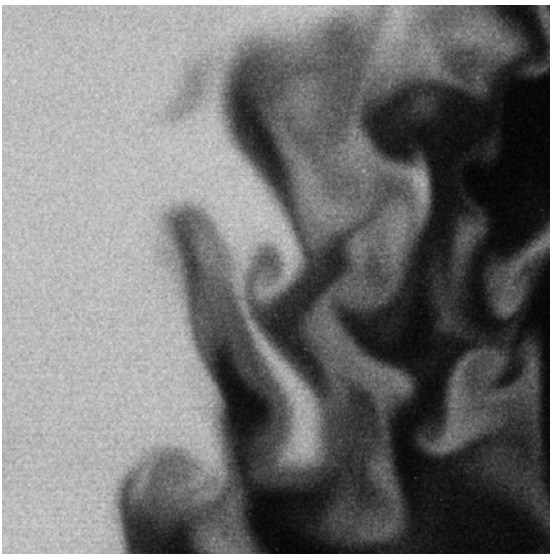


Fig. 3: Single shot tracer LIF with homogenized excitation beam profile. Mixing between unseeded ambient air (black) and seeded jet-flow (white)

By relating the single shot measurement to an average image of Rayleigh scattering on homogeneous ambient air, correction for the remaining inhomogeneities was performed. An exemplary single shot image of a turbulent mixing experiment is shown in Fig. 3, whereby it is worth to mention that here no correction or image processing has been performed for that image.

The homogenised rectangularly shaped beam is focused by a $f=750$ mm plan-convex lens towards the nozzle exit.

The green and UV light sheets are superposed by a dichroic mirror which is highly reflective for 248 nm and highly transmissive for 532 nm at a distance 300 mm from the nozzle exit.

A gas tracer with a normal boiling point lower than 0°C and a volumetric content of several ppm was used here. It is currently under investigation for different purposes and planned for publication

in form of a patent, hence it is not named here. The tracer is excited at 248 nm by a KrF-excimer laser with a maximum pulse energy of 250 mJ/pulse. Diffusive transport of the tracer out of inner jet flow was calculated to be negligible compared to convective transport. Therefore, the mixture fraction defined in terms of the inner flow mass fraction can directly be derived from the fluorescence signal of the tracer substance. The red-shifted fluorescence signal between 260 and 350 nm was imaged by an UV-sensitive 105 mm f/4.5 Nikon Nikkor objective onto the chip of a double-intensified CCD camera. In order to lower the read-out noise, a 2×2 quadratic binning of the pixels is applied which results in an effective size of the images of 512×512 pixels. Rayleigh scattering at the excitation wavelength was eliminated by an UG11 high-pass filter.

Preliminary to the actual measurement of the simultaneous flow- and mixture fraction field, the dependency of the mixture fraction on the detectable signal is investigated by performing a calibration for six different tracer concentrations directly at the burner outlet where the mixture fraction is maximum (Fig. 4).

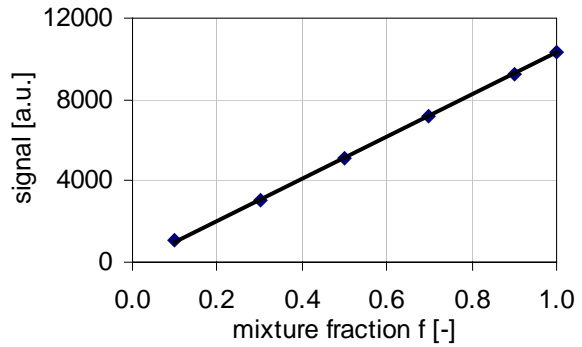


Fig. 4: Signal calibration

3. Results

In the following, the results of the simultaneous detection of velocity and mixture fraction inside the turbulent jet flow for $Re=31714$ are presented for three different downstream positions being located in the jet core, the transition region and the region of beginning self-similarity. With the aim to keep the resulting data-set clearly arranged, the quantities are shown in profile view for $x/D=0.5$, 6.0 and 11.0.

Unlike other studies, where profiles of measured flow and scalar fields are presented, starting from the symmetry axis towards merely a single radial direction, we depict our data-set for both radial directions. Thus, a perfect comparison to numerical calculations is enabled, as the lowest data-set can serve as an inlet condition for numerical studies which incorporates possible unavoidable remaining asymmetries of the measurement setup. For the case of assumed but not explicitly shown symmetry, the difference between the numerical study and the experiment will be large, if the numerical study assumes symmetry whereas the experiment is slightly asymmetric.

First, the spatially averaged axial velocity profiles are displayed in Fig. 5. The measured profiles taken at different heights above the outlet follow the free jet theory. Close to the outlet the profile is similar to a turbulent plug flow, with high gradients inside the shear layer. After passing the transition zone for $x/D=6$, the jet breaks down with further downstream position, resulting in a typical flattening and broadening of the profile in the starting self-similarity zone ($x/D=11$).

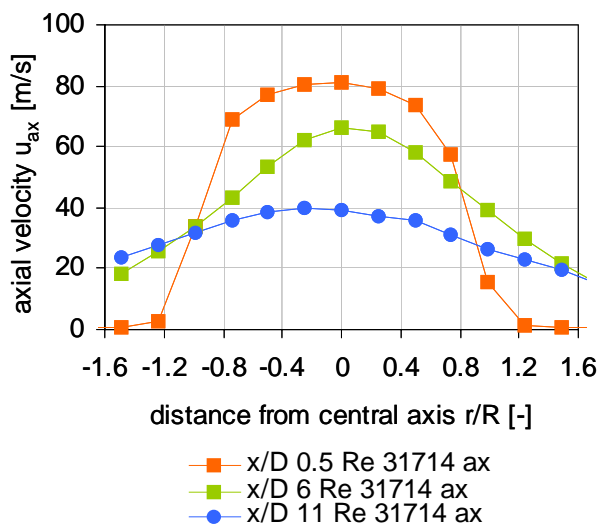


Fig. 5. Ensemble averaged filtered axial velocity

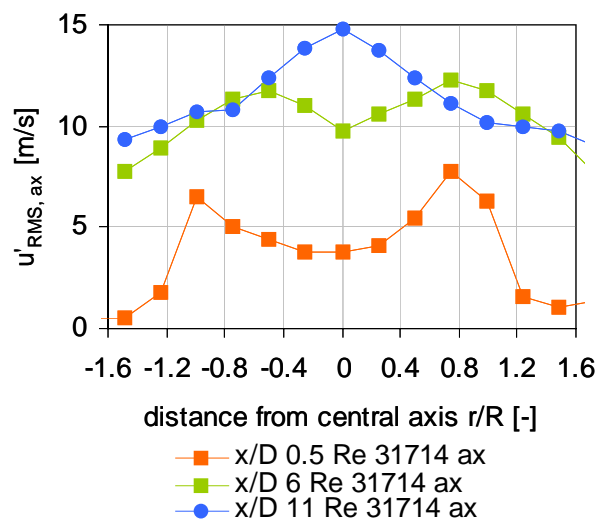


Fig. 6. RMS fluctuation of the ensemble averaged filtered axial velocity

The influence of the shear layer on the profile of the RMS values of the axial velocity fluctuations is displayed in Fig. 6. Especially for the jet core ($x/D=0.5$), the highest fluctuations are located above the rim. With further downstream position the axial turbulent fluctuations increase towards the beginning self-similarity region ($x/D=11$), where the turbulence starts to decay.

Also the profiles of the ensemble averaged mixture fraction in Fig. 7 characterize the typical zones of a free jet, similar to the profiles of the averaged axial velocity. Though, the distribution for the jet core ($x/D=0.5$) is closer to a flat-top profile as the mixture fraction is not influenced by the shear layer here. The effect of entrainment of ambient air typically starts in the transition zone ($x/D=6$). The profiles for the RMS values of the mixture fraction fluctuation (Fig. 8) are similar to that of the axial velocity. However, turbulent transport has degraded the mean value of mixture fraction at

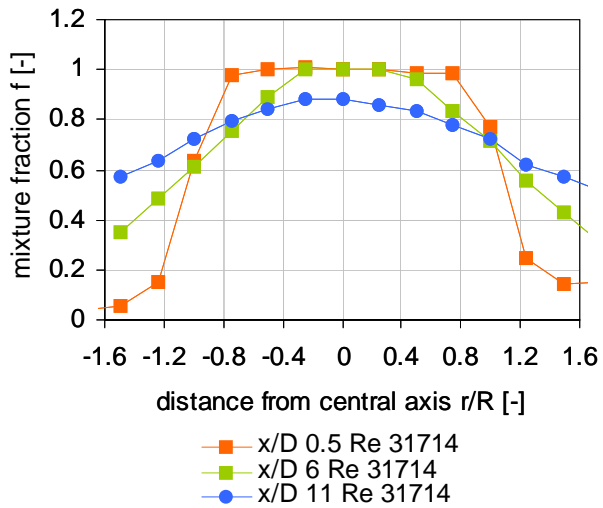


Fig. 7. Ensemble averaged mixture fraction

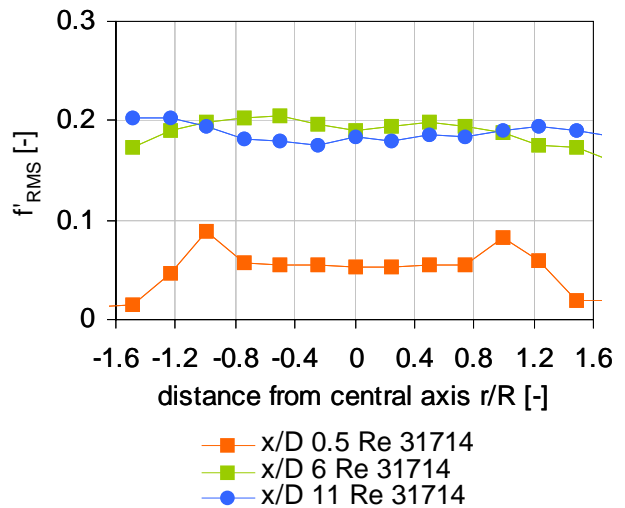


Fig. 8. RMS fluctuation of the ensemble averaged mixture fraction

$x/D=11$ in such a manner, that the resulting fluctuations are smaller than that in the transition zone, whereby the fluctuations of the velocity are highest in the beginning self-similarity zone.

The difference between the development of mixture fraction and the flow-field gets clearer when spatial correlation characteristics of the regarding properties are compared. For this purpose, in

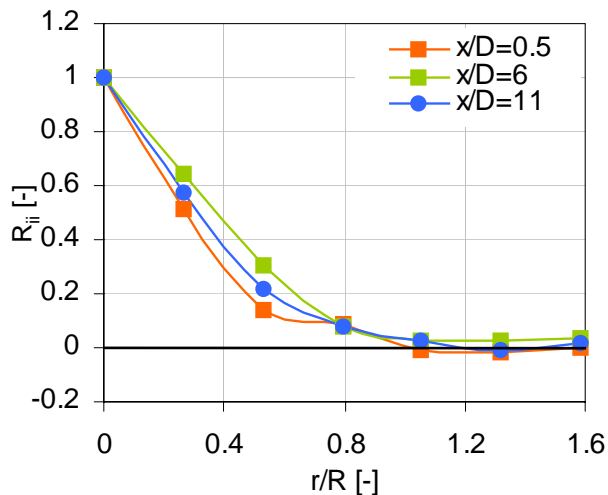


Fig. 9: Transversal correlation of the axial velocity component starting from $r/R = 0$

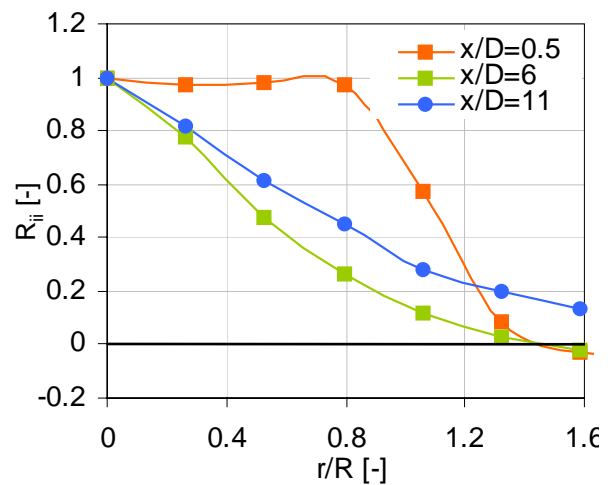


Fig. 10: Radial correlation of the mixture fraction starting from $r/R = 0$

Figs. 9 and 10, the correlation coefficients of the axial velocity and the mixture fraction are plotted as a function of the radial distance, starting from the central axis.

The effects of entrainment and turbulent mixing are clearly visible in the correlation plot of the mixture fraction (Fig. 10). The referring plots for $x/D=6$ and 11 are obviously less steep as a result from the simultaneous dilution by ambient air and mixing effects. The first three points for the plot at $x/D=0.5$ seem to be atypical for correlations characteristics, however, they exhibit high similarity as no dilution affects the mixture fraction field inside the jet core. In contrast, the correlation coefficients for the axial velocity component (Fig. 9) feature a faster decay in radial direction, with little differences when the different downstream positions are regarded. The radial similarity of the axial component is lowest for $x/D=0.5$.

The instantaneous correlation and spatial filtering of the mixture fraction and velocity according to Eq. (7) allows to evaluate the SGS scalar flux. This is, to the best of the authors knowledge, the first experimental study on that term. The respective profiles are depicted in Fig. 11. Obviously, the SGS

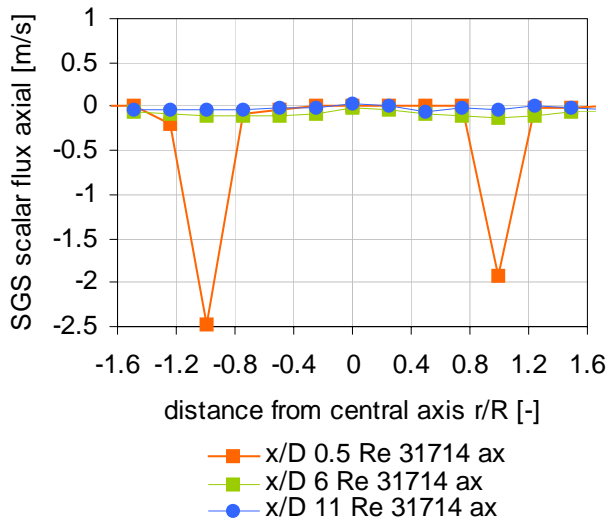


Fig. 11. Ensemble averaged SGS scalar flux - measured

scalar flux is maximum inside the shear layer of the jet core ($x/D=0.5$), with a strong decrease further downstream.

The quality of the models for the SGS scalar flux can now be assessed by direct comparison with the presented profile data, which is the primary aim of the study. Moreover, it is possible from the persisting data-set to directly evaluate the model prediction from the experimental data. As mentioned in Eq. (7), the SGS scalar flux is usually modeled by a standard gradient approach together with the Smagorinsky model for the turbulent viscosity $\tilde{\nu}_t$. Here, the gradient of the mixture fraction $\partial \tilde{f} / \partial x_i$ is directly accessible from spatial filtering of the instantaneous mixture fraction. Following this model, the turbulent viscosity is derived from the absolute value of the

deformation tensors $|\tilde{S}_{ij}|$. As in Eq. (6c) the velocity gradients appear for all three directions in space, whereby the planar measurement only allows to derive in-plane gradients (indices $11, 12, 21, 22$), the missing five components of the tensor have to be estimated by a model assumption. One possibility is to assume axis-symmetry with regard to the main flow direction (index 2) combined with symmetry condition of the not accessible components (Eq. (11)). In the second approach, the total amount of the deformation tensor is scaled proportional to the number of its accessible

I. assumption of symmetry:
$$|S_{ij}| = \sqrt{2} \left(2S_{11}^2 + S_{22}^2 + 6S_{12}^2 \right)^{0.5} \quad (11)$$

II. assumption of proportionality:
$$|S_{ij}| = \sqrt{2} \cdot \sqrt{9/4} \cdot \left(S_{11}^2 + S_{22}^2 + 2S_{12}^2 \right)^{0.5} \quad (12)$$

components (Eq. (12)).

In order to estimate the validity of both assumptions, a LES case study of a cold burner chamber with an exit velocity of 45 m/s was performed (Fig. 12). The resulting minimal and maximal values of the deformation tensor based on both assumptions and the direct numerical evaluation are summarized in Table 1.

The 2nd assumption shows good agreement with the directly evaluated deformation tensor for that case. Therefore, the 2nd assumption is applied in order to calculate the total amount of the spatially filtered deformation tensor from the planar measurements.

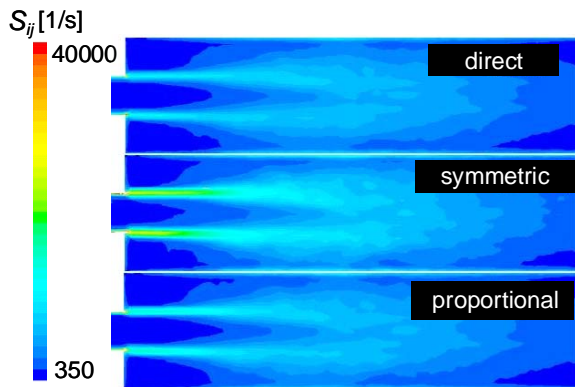


Table 1: Results of the numerical case study

$ \tilde{S}_{ij} $	min. value [1/s]	max. value [1/s]
direct simulation	350	64930
I. assumption of symmetry	451	98968
II. assumption of proportionality	376	67937

Fig. 12: LES case study on the deformation tensor S_{ij}

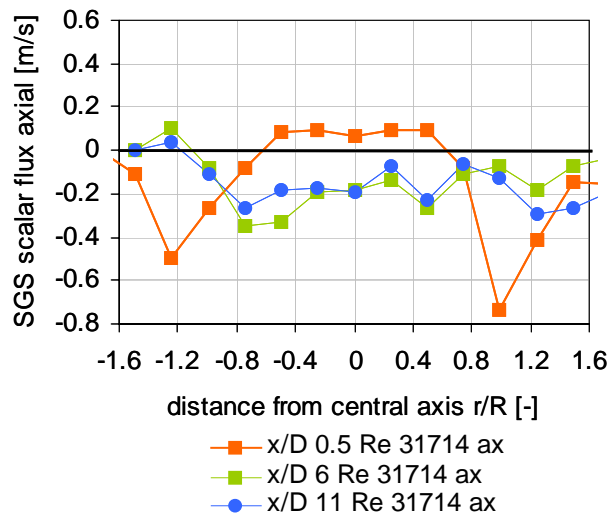


Fig. 13. Ensemble averaged SGS scalar flux – Smagorinsky model

Thus the SGS scalar flux derived according to the standard gradient approach is accessible from the measured data set by a combined evaluation of the spatially filtered gradient of the mixture fraction and the application of the Smagorinsky model for the turbulent viscosity (Fig. 13). At first glance, the profile is noisier, which is a direct result from the noise-enhancing numerical formation of local gradients. However, the trend to decreasing absolute values with further downstream position is also noteworthy. Similar to the direct measurement, the maximum is located close to the outlet, though the absolute value seems to be underpredicted by the gradient model.

4. Summary

An experimental strategy for the simultaneous two-dimensional measurement of mixture fraction and flow velocity of a non-reacting jet flow is presented in this study. By instantaneously applying planar laser-induced fluorescence and particle image velocimetry, data for the validation of models used in large eddy simulations are provided. The requirement for validation of simultaneous filtered and sub-grid data was fulfilled by performing the experiments with high spatial resolution of $110 \mu\text{m}$ spacing between adjacent regions of interest. Therefore, special measures were taken in order to access velocities in the range of $\text{Ma} \approx 0.2$. Furthermore, several strategies are presented in order to perform tracer based planar LIF techniques quantitatively. In this context, quenching effects of the fluorescing molecules have no influence on the quantification process of the mixture fraction with regard to maximum concentration of the jet flow, as both the jet- as well as the co-flow feature the same molecular composition and temperature. Subsequent to a calibration procedure at the nozzle exit, the mixture fraction is calculated, whereby a number of steps are taken in order to exclude influences from intensity fluctuations of the total laser output energy and inhomogeneous illumination of the object plane. The turbulent jet is characterized at three different

downstream positions which cover the jet core, the transition region and the beginning region of self-similarity. The referring profile data of ensemble averaged axial velocity, axial RMS velocity fluctuations, mixture fraction and RMS fluctuations of the mixture fraction are depicted on a spatially averaged database over 81 subscale ROIs. Besides those first order moments, spatial correlation characteristics of the mixture fraction and the axial velocity are evaluated in radial direction, starting from the jet central axis. It could be shown, that the mixture fraction field seems to develop faster towards the region of self similarity than the flow-field as a result of turbulent mixing and entrainment of ambient air. The demonstrated direct measurement of the subgrid-scale scalar flux by simultaneously measuring vector and scalar quantities via spatially filtering of instantaneous correlations, depicts a novel way for providing experimentally accessed data-sets for the validation of models used in computational fluid dynamics. Here, the first experimental results of the SGS scalar flux of a free jet are shown. The axial SGS scalar flux was measured to be maximal close to the nozzle exit. Moreover, besides the direct measurement, the experimental data-set allows to directly evaluate model predictions, e.g., the standard gradient approach for the SGS scalar flux. For this direct comparison, a preceding numerical case study was performed, with the aim to validate theoretical assumptions for accessing the complete three-dimensional deformation tensor from the planar velocity field measurement. A first comparison with the aforementioned direct measurement of the axial SGS scalar flux shows, that the standard gradient approach seems to underpredict the scalar flux in axial direction of the investigated jet flow close to the nozzle exit. However, resulting from the noise enhancing multiplication of mixture fraction gradients with the total amount of the strongly gradient dependent deformation tensor, a direct comparison of both approaches seems to be advisable only qualitatively.

5. Acknowledgments

The authors gratefully acknowledge the financial support of parts of this work from the German Science Foundation (DFG) and from the Bavarian Research Cooperation FORTVER, hosted by the Arbeitsgemeinschaft der Bayerischen Forschungsverbände (abayfor). For the execution of the numerical case study and fruitful discussions on the field of large eddy simulation we dedicate special thank to our former colleague Naresh Aluri, now with the Lehrstuhl für Thermodynamik und Verbrennung, Universität Siegen.

6. References

- Branley N, Jones W P (2001) Large Eddy simulation of a turbulent non-premixed flame. *Comb. Flame* 127(1-2):1914-1934
- Chen J-Y, Dibble R W, Bilger R W (1990) PDF Modeling of Turbulent Non-Premixed CO/H₂/N₂ Jet Flames with Reduced Mechanisms. *Proc. Combust. Inst.* 23:775
- Cook A W, Riley J J (1998) Subgrid-Scale Modeling for Turbulent Reacting Flows. *Comb. Flame* 112:593-606
- Forkel H, Janicka J (2000) Large-Eddy simulation of a turbulent hydrogen diffusion flame. *Flow Turbul. Combust.* 65:163-175
- Hart D P (1998) The Elimination of Correlation Errors in PIV Processing. In: *Proc 9th International Symposium on Applications of Laser Techniques to Fluid Mechanics, Lisbon, Portugal*
- Hinze J O (1962) *Turbulence*. McGraw-Hill, New York
- Jaberi F A, Colucci P J (2003) Large Eddy Simulation of heat and mass transport in turbulent flows. Part 2: Scalar field. *Int. J. Heat Mass Tran.* 46:1827-1840
- Jimenez C, Dopazo C, Valino L (2000) Application of an Eulerian Monte Carlo field method to the simulation of the filtered PDF in LES. In: *Proc 8th European Turbulence Conference, Barcelona, Spain*, pp 223-226
- Kerstein A R (1988) Linear-Eddy modeling of turbulent scalar transport and mixing. *Combust. Sci. and Tech.* 60:391-421
- Lilly D K (1992) A proposed modification of the germano subgrid-scale closure method. *Phys. Fluids A* 4(3):633-635

- Meneveau C, Katz J (2000) Scale-invariance and turbulence models for large-eddy simulation. *Annu. Rev. Fluid. Mech.* 32:1-32
- Pfadler S, Löffler M, Dinkelacker F, Leipertz A (2005) Measurement of the conditioned turbulence and temperature field of a premixed Bunsen burner by planar laser Rayleigh scattering and stereo particle image velocimetry. *Exp. Fluids* 39:375-384
- Pitsch H, Steiner H (2000) Large-Eddy simulation of a turbulent piloted methane/air diffusion flame (Sandia flame D). *Phys. Fluids* 10(12):2541-2554
- Pitsch H, Steiner H (2000) Scalar Mixing and Dissipation Rate in Large-Eddy Simulations of Non-Premixed Turbulent Combustion. *Proc. Combust. Inst.* 28:41
- Ronneberger O, Raffel M, Kompenhans J (1998) Advanced evaluation algorithms for standard and dual plane particle image velocimetry. In: *Proc 9th international symposium on applications of laser techniques, Lisbon, 13. - 16.7., pp 10.1*
- Smagorinsky J (1963) General circulation experiments with the primitive equations. *Mon. Weather Rev.* 91:99-164
- Speziale C G, Erlebacher G, Zang T A, Hussaini M Y (1988) On the subgrid-scale modeling of compressible turbulence. *Phys. Fluids* 31:940-942
- Steiner H, Bushe W K (2001) Large eddy simulation of a turbulent reacting jet with conditional source-term estimation. *Phys. Fluids* 13(3):754-769
- Stolz S, Adams N A (1999) An approximate deconvolution procedure for Large-Eddy simulation. *Phys. Fluids A* 11(7):1699-1701
- Wegner B, Kempf A, Sadiki A, Janicka J (2002) Large Eddy Simulation of Combustion Systems under Gas Turbine Conditions. In: *Proc 1st International Workshop on Trends in Numerical and Physical Modelling for Tubulent Processes in Gas Turbine Combustors, Darmstadt, Germany, 14-15 November.*